A&A 448, L43–L47 (2006)
DOI: 10.1051/0004-6361:200600014

Astronomy & Astrophysics

First detection of a VHE gamma-ray spectral maximum from a cosmic source: HESS discovery of the Vela X nebula

F. Aharonian[1], A. G. Akhperjanian[2], A. R. Bazer-Bachi[3], M. Beilicke[4], W. Benbow[1], D. Berge[1], K. Bernlöhr[1,5], C. Boisson[6], O. Bolz[1], V. Borrel[3], I. Braun[1], F. Breitling[5], A. M. Brown[7], R. Bühler[1], I. Büsching[8], S. Carrigan[1], P. M. Chadwick[7], L.-M. Chounet[9], R. Cornils[4], L. Costamante[1,21], B. Degrange[9], H. J. Dickinson[7], A. Djannati-Ataï[10], L. O'C. Drury[11], G. Dubus[9], K. Egberts[1], D. Emmanoulopoulos[12], B. Epinat[13], P. Espigat[10], F. Feinstein[13], E. Ferrero[12], G. Fontaine[9], Seb. Funk[5], S. Funk[1], Y. A. Gallant[13], B. Giebels[9], J. F. Glicenstein[14], P. Goret[14], C. Hadjichristidis[7], D. Hauser[1], M. Hauser[12], G. Heinzelmann[4], G. Henri[15], G. Hermann[1], J. A. Hinton[1,12], W. Hofmann[1], M. Holleran[8], D. Horns[16], A. Jacholkowska[13], O. C. de Jager[8], B. Khélifi[9,1], Nu. Komin[5], A. Konopelko[5], I. J. Latham[7], R. Le Gallou[7], A. Lemière[10], M. Lemoine-Goumard[9], T. Lohse[5], J. M. Martin[6], O. Martineau-Huynh[17], A. Marcowith[3], C. Masterson[1,21], T. J. L. McComb[7], M. de Naurois[17], D. Nedbal[18], S. J. Nolan[7], A. Noutsos[7], K. J. Orford[7], J. L. Osborne[7], M. Ouchrif[17,21], M. Panter[1], G. Pelletier[15], S. Pita[10], G. Pühlhofer[12], M. Punch[10], B. C. Raubenheimer[8], M. Raue[4], S. M. Rayner[7], A. Reimer[19], O. Reimer[19], J. Ripken[4], L. Rob[18], L. Rolland[14], G. Rowell[1], V. Sahakian[2], L. Saugé[15], S. Schlenker[5], R. Schlickeiser[19], U. Schwanke[5], H. Sol[6], D. Spangler[7], F. Spanier[19], R. Steenkamp[20], C. Stegmann[5], G. Superina[9], J.-P. Tavernet[17], R. Terrier[10], C. G. Théoret[10], M. Tluczykont[9,21], C. van Eldik[1], G. Vasileiadis[13], C. Venter[8], P. Vincent[17], H. J. Völk[1], S. J. Wagner[12], and M. Ward[7]

(Affiliations can be found after the references)

Received 20 December 2005 / Accepted 24 January 2006

ABSTRACT

The Vela supernova remnant (SNR) is a complex region containing a number of sources of non-thermal radiation. The inner section of this SNR, within 2 degrees of the pulsar PSR B0833−45, has been observed by the HESS γ-ray atmospheric Cherenkov detector in 2004 and 2005. A strong signal is seen from an extended region to the south of the pulsar, within an integration region of radius 0.8° around the position ($\alpha = 08^{\rm h}35^{\rm m}00^{\rm s}$, $\delta = -45°36'$ J2000.0). The excess coincides with a region of hard X-ray emission seen by the ROSAT and ASCA satellites. The observed energy spectrum of the source between 550 GeV and 65 TeV is well fit by a power law function with photon index $\Gamma = 1.45 \pm 0.09_{\rm stat} \pm 0.2_{\rm sys}$ and an exponential cutoff at an energy of $13.8 \pm 2.3_{\rm stat} \pm 4.1_{\rm sys}$ TeV. The integral flux above 1 TeV is $(1.28 \pm 0.17_{\rm stat} \pm 0.38_{\rm sys}) \times 10^{-11}$ cm^{-2} s^{-1}. This result is the first clear measurement of a peak in the spectral energy distribution from a VHE γ-ray source, likely related to inverse Compton emission. A fit of an Inverse Compton model to the HESS spectral energy distribution gives a total energy in non-thermal electrons of $\sim 2 \times 10^{45}$ erg between 5 TeV and 100 TeV, assuming a distance of 290 parsec to the pulsar. The best fit electron power law index is 2.0, with a spectral break at 67 TeV.

Key words. ISM: plerions, Gamma rays: observations

1. Introduction

The region surrounding the Vela supernova remnant (SNR) is very well studied across the electromagnetic spectrum and contains a number of complex objects, including the SNR RX J0852.0−4622, which has been previously detected in the very high energy γ-ray (VHE) range (Katagiri et al. 2005; Aharonian et al. 2005b). The Vela SNR itself, at a distance estimated to be ∼290 pc (Dodson et al. 2003; Caraveo et al. 2001), extends over a diameter of ∼8°. It is the nearest SNR to contain a young active pulsar, PSR B0833−45, with a period of 89 ms and a period derivative $\dot{P}$ of 1.25×10^{-13} s s^{-1}. This implies a spin-down luminosity of 7×10^{36} erg s^{-1} and age of 11 000 years. Observations by Chandra (Helfand et al. 2001) clearly show the torus-like morphology of the compact X-ray nebula surrounding the pulsar and have allowed its rotation axis to be inferred. The plane of the torus (i.e. pulsar equator) appears to intersect the plane of the sky at a position angle of 40.6° relative to North (Ng & Romani 2004), and its X-ray spectral index of ∼1.5 (Mangano et al. 2005) is typical of pre-cooled pulsar wind torii.

The SNR also contains a number of regions of non-thermal emission, including those labelled by Rishbeth (1958) from radio observations as Vela X, Vela Y and Vela Z (which is part of the shell of RX J0852.0−4622). A diffuse emission feature

has been detected by ROSAT (Markwardt & Ögelman 1995) in hard X-rays (0.9−2.0 keV), coinciding with the centre of the Vela X region. It was first suggested that this feature, which is aligned closely with a filament detected at radio wavelengths, corresponds to the outflow jet from the pole of the pulsar (Frail et al. 1997). However, the Chandra observations showed that this feature lies along the extension of the pulsar equator, although bending to the southwest.

The study of Vela X is important from two perspectives: It was the first middle-aged pulsar wind nebula (PWN) to be detected, thereby introducing the concept of PWN evolution (Weiler & Panagia 1980). Also, it served as the first prototype for offset PWN as a result of SNR expansion into an inhomogeneous medium (Blondin et al. 2001), of which G18.0-0.7 served as a second example (Gaensler et al. 2003). This second PWN was also recently identified with VHE source HESS J1825−137 (Aharonian et al. 2005c).

Here we discuss observations of the Vela pulsar and the centre of the Vela SNR with HESS, including the Vela X feature. A region of extended γ-ray emission is detected, to the south of the pulsar position (previously reported by Khélifi et al. (2005). This region was previously observed by the CANGAROO collaboration (Yoshikoshi et al. 1997) and emission of VHE γ-rays was claimed from a source 0.13° to the southeast of the pulsar. However doubt was later cast on the significance of this detection (Dazeley et al. 2001). A recent paper from the CANGAROO collaboration (Enomoto et al. 2005) retracts the claimed detection, and suggests some evidence for an excess coincident with the HESS signal.

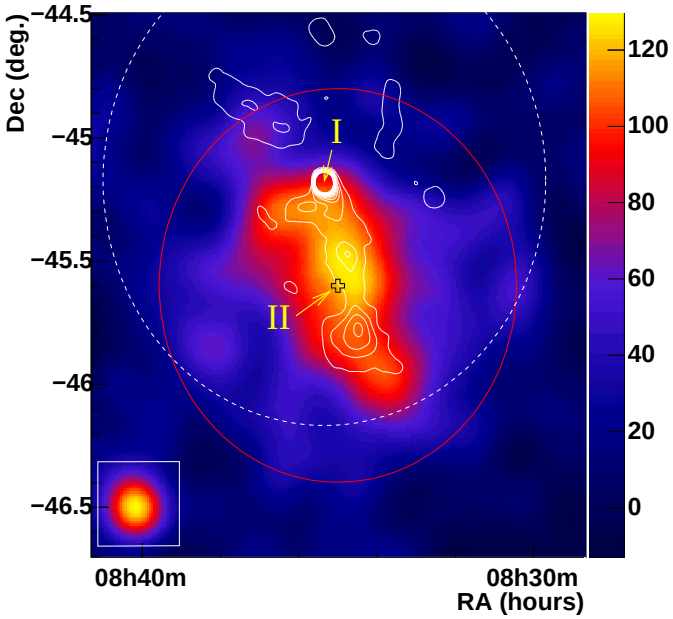

Fig. 1. Gaussian smoothed sky map of region surrounding Vela pulsar, showing significant emission to the south of the pulsar position, coincident with an X-ray feature seen by ROSAT (white contours). The smoothing width used is 0.09°. The contours corresponding to the strong emission close to the pulsar (position I) are truncated. The image inset in the bottom left corner indicates the size of a point source as seen by HESS, for an equivalent analysis. The solid circle represents the HESS integration region for the spectral measurement, while the dashed circle represents the field of view for the ROSAT observations. Position II is marked by a black cross.

2. Observations with HESS

HESS is a system of four atmospheric Cherenkov telescopes designed to look for astrophysical γ-ray emission above ∼100 GeV; a review of the detector is given by Hinton (2004). The Vela region was observed between January and March 2004 with the complete HESS array. In total 10.3 h of data were obtained, after standard data quality selection, at zenith angles between 20° and 40°. These observations were taken using a method (*wobble* mode) whereby the source is offset by a small angular distance from the centre of the field of view, alternating between 28 min runs in the positive and negative declination (or right ascension) directions. The observations were made at offsets of 0.5° in declination from the position of the Vela pulsar, ($\alpha = 08^{\rm h}35^{\rm m}20^{\rm s}$, $\delta = -45°10'35''$ J2000.0), which is referred to as position I for the purposes of this paper.

Following a detection of extended γ-ray emission to the south of the pulsar in the 2004 dataset, further observations were made in 2005 surrounding the position $\alpha = 08^{\rm h}35^{\rm m}00^{\rm s}$, $\delta = -45°36'$ (J2000.0), here referred to as position II, which was measured as the centre of gravity of the excess. These were also taken in wobble mode, and the mean offset for the 2005 data is 0.5°. After data quality selection 7.2 h of observations were available for analysis, giving total observation live time over the two years of 16.4 h, after dead time correction (approximately 10%). The mean zenith angle for the complete set of observations is 30.2°.

3. Analysis

The observations of the Vela region were calibrated using standard HESS calibration procedures, as discussed by Aharonian et al. (2004) and analysed using the *scaled width* method, as discussed by Aharonian et al. (2005a). The *hard* cuts, as defined in the latter paper were applied to this source. These cuts improve the angular resolution and reduce systematic effects due to uncertainties in the background estimation, relative to the standard cuts, albeit at the expense of a higher than usual energy threshold (450 GeV for the analysis presented here).

The background level in this analysis was estimated using the *on-off* method, based on a sample of runs taken at similar zenith angles (external to the Vela SNR) which contain no excess γ-ray signal. This method allows the background level to be estimated in cases where the integration region for the source is comparable to the size of the field of view. The off runs are carefully chosen to match well the on source observations in zenith angle and system configuration.

Figure 1 shows a sky map of the excess in the region south of the Vela pulsar. The map has been smoothed with a Gaussian function with a sigma of 0.09° and is not corrected for variations in the γ-ray radial acceptance of the detector, which are less than 10% across the integration region. Position II, as defined above, is marked by a black cross. The extent and position of the excess has been determined by fitting a two dimensional, elongated Gaussian, convolved with the point spread function of the instrument for these

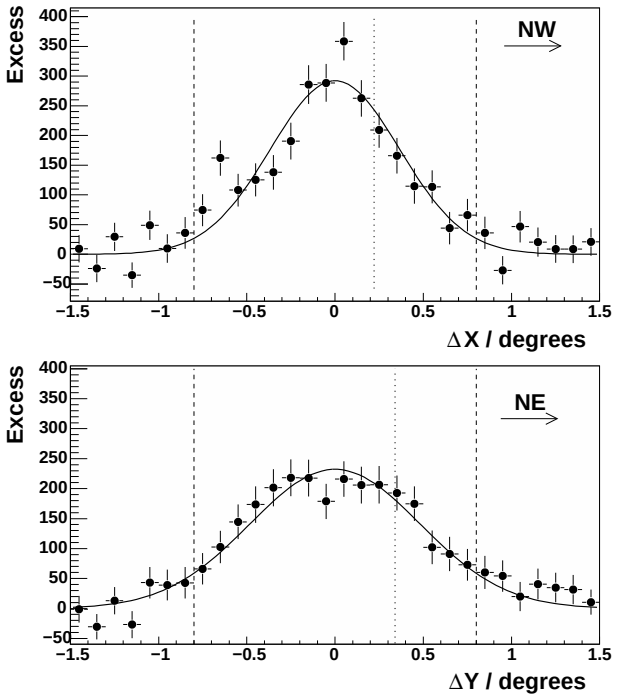

Fig. 2. Profile of the excess from the extended feature coincident with Vela X along minor axis (*top*) and along major axis (*bottom*); events within 0.8° of the axis are integrated into the profile in each case. The two dimensional fit of an elongated Gaussian convolved with the HESS PSF is also shown as a profile for comparison. The position of the Vela pulsar is marked by a vertical dotted line in each plot for reference, while the integration region in each case for the spectral measurement is marked by dashed lines (within 0.8° of position II).

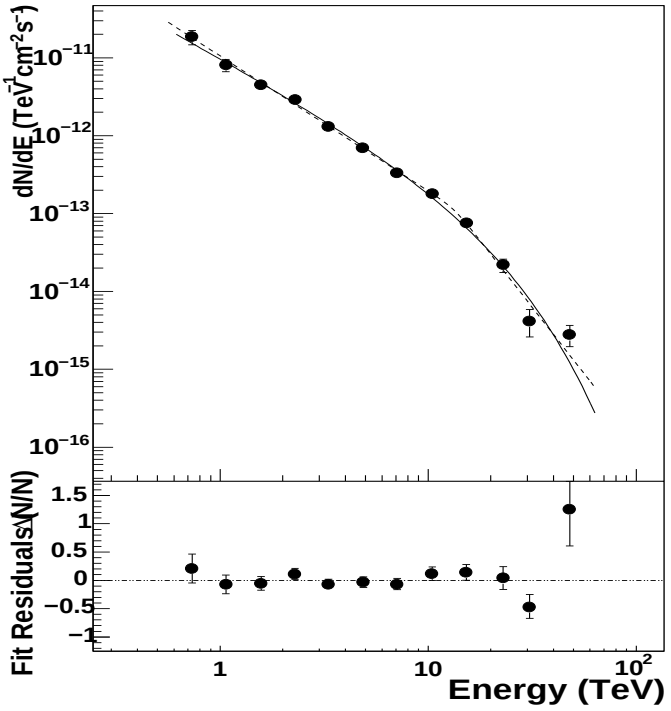

Fig. 3. Energy spectrum of γ-ray emission from the Vela X region. The solid line denotes the best fit of a power law with an exponential cutoff. The dashed line represents the best fit broken power law spectrum. The bottom panel shows the residuals to the exponential cutoff fit.

measurements, which is 0.08° (68% containment radius), to an uncorrelated excess map of the source. The best fit intrinsic width along the major axis is 0.48° ± 0.03°, while the best fit intrinsic width along the minor axis is 0.36° ± 0.03°. The major axis of the fitted distribution is at a position angle of 41° ± 7°. The best-fit centre of gravity of the emission region (α = 08$^{\rm h}$35$^{\rm m}$1$^{\rm s}$, δ = −45°34′40″ J2000.0) is consistent with position II, within the statistical error of 2 arcmin. The VHE source is thus identified as HESS J0835−455.

Profiles of the excess parallel to, and perpendicular to, the major axis of the fit are shown in Fig. 2. Profiles of the elongated Gaussian fit are shown for comparison. It can be seen that, given the statistical errors in each bin, the elongated Gaussian fits the excess well, with a χ^2 of 277.8 for 250 degrees of freedom. A circular Gaussian fit to the same excess gives a width of 0.43° ± 0.02°, with a χ^2/d.o.f. of 290.0/252.

The radius of the integration region used for estimating the flux and spectrum of the VHE emission was 0.8°, surrounding position II, as defined above. This size was chosen so as to encompass the entire excess, as seen in Fig. 1. A total of 9610 *on*-source counts and 7879 *off*-source counts were detected above 450 GeV, with a normalisation factor of 0.94 between the *on* and *off* observations, giving an excess of 2152 events within the integration region. The statistical excess significance is 16.7σ, calculated using the method described by Li & Ma (1983).

Figure 3 shows the energy spectrum of the signal seen from the integration region. The spectrum is well fit (with a χ^2/d.o.f. of 13.1/10) by a power law function with photon index $\Gamma = 1.45 \pm 0.09_{\rm stat} \pm 0.2_{\rm sys}$ and an exponential cutoff at an energy of $13.8 \pm 2.3_{\rm stat} \pm 4.1_{\rm sys}$ TeV. The data may alternatively be described using a broken power law function, with a spectral break at $13.4 \pm 3.1_{\rm stat} \pm 4.1_{\rm sys}$ TeV and photon index of $\Gamma_1 = 1.7 \pm 0.1_{\rm stat} \pm 0.2_{\rm sys}$ at lower energies hardening to $\Gamma_2 = 3.4 \pm 0.7_{\rm stat} \pm 0.2_{\rm sys}$ above the break energy. The χ^2/d.o.f. of the broken power law fit, which includes a term for the width of the transition region, is 9.0/8. A straight power law fit (χ^2/d.o.f. of 74.1/11) is rejected. The integral flux above 1 TeV (from the exponential cutoff fit) is $(1.28 \pm 0.17_{\rm stat} \pm 0.38_{\rm sys}) \times 10^{-11}$ cm^{-2} s^{-1}. The systematic error on the flux estimation is estimated at 30%, mainly due to uncertainties in the transparency of the atmosphere to Cherenkov light. In fitting the energy spectrum for this source, the energy of each event is corrected for the detector optical efficiency, relative to that used in Monte Carlo simulations to estimate the effective area of the instrument. The optical efficiency is estimated from single muon events detected during each observation run (Leroy et al. 2003; Bolz 2004). The mean energy correction is ~20%.

In order to test for a point source component in VHE γ-rays from position I (the pulsar position, as marked in Fig. 2), the residual excess within 0.1° from the pulsar, after subtraction of the Gaussian fit to the extended excess, has been measured. No significant excess after subtraction is seen, and a 99.9% upper limit on the integral flux above 1 TeV, assuming a point source at the position of the pulsar, is 7.6×10^{-13} cm^{-2} s^{-1}.

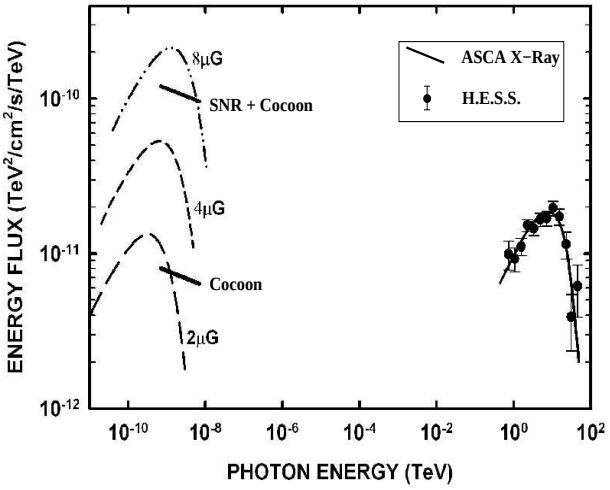

Fig. 4. Spectral energy distribution for the HESS and ASCA spectral measurements (Markwardt & Ögelman 1997). The two alternative X-ray spectra are described in the text. The fitted inverse Compton emission (solid line) from the Vela X region is shown, given the electron energy distribution described in the text. The predicted synchrotron flux is shown for three possible magnetic field levels, between 2 μG and 8 μG.

4. Discussion

The new VHE source reported here, HESS J0835–455, is situated to the south of the pulsar and the compact X-ray nebula (as seen by Chandra). The integral flux is estimated to be ∼50% of that of the Crab nebula above 1 TeV. As the distance to the pulsar is well measured, one can estimate the size of the emission region seen by HESS to be 5.1 parsec (full length for 68% containment) along the major axis by 3.8 parsec (full width). The luminosity of the emission region in the energy range from 550 GeV to 65 TeV can be estimated to be $L = 9.9 \times 10^{32}$ erg s^{-1}, using the power law fit to the spectrum with the exponential cutoff.

HESS J0835–455 appears to be spatially coincident with the X-ray (0.4−2.4 keV) emission as seen by ROSAT (shown in Fig. 1). It has been suggested (Blondin et al. 2001) that the Vela X feature corresponds to the pulsar wind nebula, displaced to the south by the unequal pressure of the reverse shock from the SNR. This hypothesis is consistent with the HESS observations which demonstrate conclusively for the first time that this feature emits non-thermal radiation. A similar explanation has been proposed for the emission seen by HESS (HESS J1825−137) close to the pulsar wind nebula G18.0–0.7 (Aharonian et al. 2005c).

The size of the feature described by Markwardt & Ögelman (1995) has been measured as 45×12 arcmin^2, whereas the VHE intrinsic size is 58×43 arcmin^2. An extension of the X-ray feature to the southwest was suggested by Lu & Aschenbach (2000), however this may be unrelated thermal emission, a suggestion which is supported by the fact that no excess is seen in this region by HESS.

The larger VHE size probably indicates that synchrotron cooling in the X-ray domain was (or still is) important. This is confirmed by the detection of a cooled X-ray photon index of ∼2.1 (Markwardt & Ögelman 1997) in the emission region, which is consistent with the uncooled photon index of 1.5 closer to the source. Figure 4 shows a spectral energy distribution (SED) for Vela X, including the HESS result reported here. Two possible X-ray spectra are shown, the lower including only the "Cocoon" feature defined in the above paper, while the upper flux includes the emission from the "SNR" component extrapolated over the HESS integration region.

A simple one-zone model of inverse Compton emission from interactions with the cosmic microwave background (CMBR) is also shown. The HESS observations show the expected peak in the IC emission; this result is the first clear measurement of such a peak at VHE energies. The total energy content in non-thermal electrons between 5 TeV and 100 TeV is 2.2×10^{45} erg, for a distance of 290 parsec. The best fit electron power law index is 2.0, with a break at 67 TeV and a post-break index of 9. The χ^2/d.o.f. of this fit is 10.2/9. In Fig. 4 three possible synchrotron spectral energy distributions are shown, for magnetic field levels in the emission region from 2 μG to 8 μG. The synchrotron distributions are not constrained by the X-ray data, a combined fit on the X-ray and γ-ray data would more closely reproduce the measured X-ray spectral slope. A magnetic field of this magnitude may be expected in the scenario of a nebula displaced from the pulsar by an asymmetric shock.

This result demonstrates the usefulness of HESS observations in clarifying the complex morphology of this source. VHE observations of inverse Compton scattering of the CMBR allow direct inference of the spatial and spectral distribution of non-thermal electrons in a PWN, independent of contamination by thermal emission or variations in the local magnetic field.

Acknowledgements. The support of the Namibian authorities and of the University of Namibia in facilitating the construction and operation of HESS is gratefully acknowledged, as is the support by the German Ministry for Education and Research (BMBF), the Max Planck Society, the French Ministry for Research, the CNRS-IN2P3 and the Astroparticle Interdisciplinary Programme of the CNRS, the UK Particle Physics and Astronomy Research Council (PPARC), the IPNP of the Charles University, the South African Department of Science and Technology and National Research Foundation, and by the University of Namibia. We appreciate the excellent work of the technical support staff in Berlin, Durham, Hamburg, Heidelberg, Palaiseau, Paris, Saclay, and in Namibia in the construction and operation of the equipment. We have made use of the ROSAT Data Archive of the Max-Planck-Institut für Extraterrestrische Physik (MPE) at Garching, Germany.

References

Aharonian, F. A., Akhperjanian, A. G., Aye, K.-M., et al. (HESS Collaboration) 2004, Astropart. Phys., 22, 109

Aharonian, F. A., Akhperjanian, A. G., Aye, K.-M., et al. (HESS Collaboration) 2005a, A&A, 430, 865

Aharonian, F. A., Akhperjanian, A. G., Bazer-Bachi, A. R., et al. (HESS Collaboration) 2005b, A&A, 437, L7

Aharonian, F. A., Akhperjanian, A. G., Bazer-Bachi, A. R., et al. (HESS Collaboration) 2005c, A&A, 442, L25

Blondin, J. M., Chevalier, R. A., & Frierson, D. M. 2001, ApJ, 563, 806

Bolz, O. 2004, Ph.D. Thesis, Karl-Ruprecht University Heidelberg http://www.ub.uni-heidelberg.de/archiv/4812

Caraveo, P. A., De Luca, A., Mignani, R. P., & Bignami, G. F. 2001, ApJ, 561, 930
Dazeley, S. A., Patterson, J. R., Rowell, G. P., & Edwards, P. G. 2001, Astropart. Phys., 15, 313
Dodson, R., Legge, D., Reynolds, J. E., & McCulloch, P. M. 2003, ApJ, 596, 1137
Enomoto, R., Tsuchiya, K., Adachi, Y., et al. 2006, ApJ, 683
Frail, D. A., Bietenholz, M. F., Markwardt, C. B., & Ögelman, H. 1997, ApJ, 475, 224
Gaensler, B. M., Schulz, N. S., Kaspi, V. M., Pivovaroff, M. J., & Becker, W. E. 2003, ApJ, 588, 441
Helfand, D. J., Gotthelf, E. V., & Halpern, J. P. 2001, ApJ, 556, 380
Hinton, J. A. 2004, New Astron. Rev., 48, 331
Katagiri, H., Enomoto, R., Ksenofontov, L. T., et al. 2005, ApJ, 619, L163
Khélifi, B., et al. 2005, in Proceedings of the 29th International Cosmic Ray Conference (Pune), 1, 101
Leroy, N., et al. 2003, in Proceedings of the 28th International Cosmic Ray Conference, Tsukuba, 1, 2895 [arXiv:astro-ph/0307452]
Li, T.-P., & Ma, Y.-Q. 1983, ApJ, 272, 317
Lu, F. J., & Aschenbach, B. 2000, A&A, 362, 1083
Mangano, V., Massaro, E., Bocchino, F., Mineo, T., & Cusumano, G. 2005, A&A, 436, 917
Markwardt, C. B., & Ögelman, H. 1995, Nature, 375, 40
Markwardt, C. B., & Ögelman, H. B. 1997, ApJ, 480, L13
Ng, C.-Y., & Romani, R. W. 2004, ApJ, 601, 479
Rishbeth, H. 1958, Austr. J. Phys., 11, 550
Weiler, K. W., & Panagia, N. 1980, A&A, 90, 269
Yoshikoshi, T., Kifune, T., Dazeley, S. A., et al. 1997, ApJ, 487, L65

[1] Max-Planck-Institut für Kernphysik, PO Box 103980, 69029 Heidelberg, Germany
[2] Yerevan Physics Institute, 2 Alikhanian Brothers St., 375036 Yerevan, Armenia
[3] Centre d'Étude Spatiale des Rayonnements, CNRS/UPS, 9 Av. du Colonel Roche, BP 4346, 31029 Toulouse Cedex 4, France
[4] Universität Hamburg, Institut für Experimentalphysik, Luruper Chaussee 149, 22761 Hamburg, Germany
[5] Institut für Physik, Humboldt-Universität zu Berlin, Newtonstr. 15, 12489 Berlin, Germany
[6] LUTH, UMR 8102 du CNRS, Observatoire de Paris, Section de Meudon, 92195 Meudon Cedex, France
[7] University of Durham, Department of Physics, South Road, Durham DH1 3LE, UK
[8] Unit for Space Physics, North-West University, Potchefstroom 2520, South Africa
[9] Laboratoire Leprince-Ringuet, IN2P3/CNRS, École Polytechnique, 91128 Palaiseau, France
[10] APC, 11 Place Marcelin Berthelot, 75231 Paris Cedex 05, UMR 7164, CNRS, Université Paris VII, CEA, Observatoire de Paris, France
[11] Dublin Institute for Advanced Studies, 5 Merrion Square, Dublin 2, Ireland
[12] Landessternwarte, Universität Heidelberg, Königstuhl, 69117 Heidelberg, Germany
[13] Laboratoire de Physique Théorique et Astroparticules, IN2P3/CNRS, Université Montpellier II, CC 70, Place Eugène Bataillon, 34095 Montpellier Cedex 5, France
[14] DAPNIA/DSM/CEA, CE Saclay, 91191 Gif-sur-Yvette, Cedex, France
[15] Laboratoire d'Astrophysique de Grenoble, INSU/CNRS, Université Joseph Fourier, BP 53, 38041 Grenoble Cedex 9, France
[16] Institut für Astronomie und Astrophysik, Universität Tübingen, Sand 1, 72076 Tübingen, Germany
[17] Laboratoire de Physique Nucléaire et de Hautes Energies, IN2P3/CNRS, Universités Paris VI & VII, 4 Place Jussieu, 75252 Paris Cedex 5, France
[18] Institute of Particle and Nuclear Physics, Charles University, V Holesovickach 2, 180 00 Prague 8, Czech Republic
[19] Institut für Theoretische Physik, Lehrstuhl IV: Weltraum und Astrophysik, Ruhr-Universität Bochum, 44780 Bochum, Germany
[20] University of Namibia, Private Bag 13301, Windhoek, Namibia
[21] European Associated Laboratory for Gamma-Ray Astronomy, jointly supported by CNRS and MPG